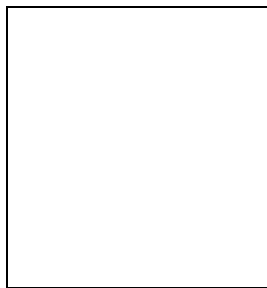


## RESULTS FROM THE $\Upsilon(5S)$ ENGINEERING RUN (BELLE)

A. DRUTSKOY

*Physics Department, University of Cincinnati, 345 Clifton Court,  
Cincinnati, OH 45221, USA*



We report results based on a  $1.86 \text{ fb}^{-1}$  data sample collected on the  $\Upsilon(5S)$  resonance by the Belle detector at the KEKB asymmetric energy  $e^+e^-$  collider. The inclusive production of  $D_s$ ,  $D^0$  and  $J/\psi$  mesons at the  $\Upsilon(5S)$  is studied. From the  $D_s$  inclusive branching fraction the ratio  $f_s = (16.4 \pm 1.4 \pm 4.1)\%$  of  $B_s^{(*)}\bar{B}_s^{(*)}$  to the total  $b\bar{b}$  quark pair production at the  $\Upsilon(5S)$  energy is obtained in a model dependent way. The exclusive decays  $B_s \rightarrow D_s^{(*)+}\pi^- (/ \rho^-)$  and  $B_s \rightarrow J/\Psi\phi (/ \eta)$  are studied and a significant  $B_s$  signal is observed combining these modes. The  $B_s$  meson production is found to proceed predominantly through the creation of  $B_s^*\bar{B}_s^*$  pairs. Upper limits on  $B_s \rightarrow K^+K^-$ ,  $B_s \rightarrow \phi\gamma$ ,  $B_s \rightarrow \gamma\gamma$  and  $B_s \rightarrow D_s^{(*)+}D_s^{(*)-}$  decays are reported.

### 1 Introduction

The possibility of studying  $B_s$  decays at very high luminosity  $e^+e^-$  colliders running at the energy of the  $\Upsilon(5S)$  resonance has been discussed in several theoretical papers<sup>1,2</sup>. In 2003 the CLEO experiment collected  $0.42 \text{ fb}^{-1}$  at the  $\Upsilon(5S)$  and observed evidence for  $B_s$  meson production in both inclusive<sup>3</sup> and exclusive<sup>4</sup> modes. However, simple calculations assuming an approximate SU(3) symmetry indicate that many interesting  $B_s$  measurements require a data sample of at least  $\sim 20 \text{ fb}^{-1}$ , which is well within the capability of the  $e^+e^- B$  factories. To test the experimental feasibility of such measurements a data sample of  $1.86 \text{ fb}^{-1}$  was recently taken at the  $\Upsilon(5S)$  energy with the Belle detector<sup>5</sup> at the KEKB<sup>6</sup> asymmetric energy  $e^+e^-$  collider. This data sample is more than four times larger than the CLEO dataset at the  $\Upsilon(5S)$ .

An energy scan was performed just before the  $\Upsilon(5S)$  data taking to define the position of the  $\Upsilon(5S)$  resonance production maximum. An integrated luminosity of  $\sim 30 \text{ pb}^{-1}$  was collected at five values of energy between 10825 MeV and 10905 MeV, at intervals of 20 MeV. Finally, the data sample of  $1.86 \text{ fb}^{-1}$  was taken at the  $\Upsilon(5S)$  energy of  $\sim 10869$  MeV. The experimental conditions of data taking at  $\Upsilon(5S)$  are exactly the same as in  $\Upsilon(4S)$  or continuum runs. The

data sample of  $3.67 \text{ fb}^{-1}$  taken in the continuum 60 MeV in CM energy below the  $\Upsilon(4S)$  is used to estimate continuum backgrounds.

## 2 Number of $b\bar{b}$ Events

In the energy region of the  $\Upsilon(5S)$  the hadronic events can be classified into three physics categories:  $u\bar{u}, d\bar{d}, s\bar{s}, c\bar{c}$  continuum events,  $b\bar{b}$  continuum events and  $\Upsilon(5S)$  events. The  $b\bar{b}$  continuum and the  $\Upsilon(5S)$  events always produce final states with a pair of  $B$  or  $B_s$  mesons and, therefore, cannot be topologically separated. We define the  $b\bar{b}$  continuum and  $\Upsilon(5S)$  events collectively as  $b\bar{b}$  events. All  $b\bar{b}$  events are expected to pass into the  $B\bar{B}, B\bar{B}^*, B^*\bar{B}^*, B\bar{B}\pi, B\bar{B}\pi\pi, B\bar{B}^*\pi, B_s\bar{B}_s, B_s\bar{B}_s^*$  or  $B_s^*\bar{B}_s^*$  final states. The excited  $B$  mesons decay to ground states via  $B^* \rightarrow B\gamma$  and  $B_s^* \rightarrow B_s\gamma$  decay channels<sup>7</sup>.

The  $u\bar{u}, d\bar{d}, s\bar{s}, c\bar{c}$  continuum subtraction method is applied to obtain the number of  $b\bar{b}$  events in the  $\Upsilon(5S)$  data sample:

$$N_{5S}^{b\bar{b}} = \frac{1}{\epsilon_{5S}^{b\bar{b}}} \left( N_{5S}^{hadr} - N_{cont}^{hadr} \times \frac{\mathcal{L}_{5S}}{\mathcal{L}_{cont}} \times \frac{E_{cont}^2}{E_{5S}^2} \times \frac{\epsilon_{5S}^{hadr}}{\epsilon_{cont}^{hadr}} \right) \quad (1)$$

Here  $N_{5S}^{b\bar{b}}$  is the number of  $b\bar{b}$  events in the  $\Upsilon(5S)$  data sample, and  $N_{5S}^{hadr}$  and  $N_{cont}^{hadr}$  are the numbers of hadronic events in the  $\Upsilon(5S)$  and continuum data samples, respectively. The efficiency to select a  $b\bar{b}$  event in the  $\Upsilon(5S)$  data sample,  $\epsilon_{5S}^{b\bar{b}} = (99 \pm 1)\%$ , and the efficiency ratio for hadronic events in the  $\Upsilon(5S)$  and continuum data samples,  $\epsilon_{5S}^{hadr}/\epsilon_{cont}^{hadr} = 1.007 \pm 0.003$ , are obtained from MC simulation. The integrated luminosity ratio  $\mathcal{L}_{5S}/\mathcal{L}_{cont}$  is calculated using a standard Belle luminosity measurement procedure based on the measurement of Bhabha events. The ratio  $\mathcal{L}_{5S}/\mathcal{L}_{cont} = 0.4740 \pm 0.0019$  is obtained after detailed calculations. From Eq. (1) we obtain the number of  $b\bar{b}$  events in the  $\Upsilon(5S)$  data sample,  $N_{5S}^{b\bar{b}} = (5.61 \pm 0.03_{stat} \pm 0.29_{syst}) \times 10^5$ . The full systematic uncertainty of  $\sim 5\%$  includes all systematic errors on parameters used in Eq. (1) and is dominated by the uncertainty on the luminosity ratio definition.

## 3 Inclusive $D_s$ Production

The method of inclusive  $D_s$  analysis of the  $\Upsilon(5S)$  data sample was developed in<sup>3</sup>. Almost the same technique is applied in this analysis. The production of  $D_s$  mesons at the  $\Upsilon(5S)$  is studied in the clean decay mode,  $D_s^+ \rightarrow \phi\pi^+$ . The  $D_s$  signals in the  $\Upsilon(5S)$  and continuum data samples are seen in Fig. 1a for the normalized  $D_s$  momentum region  $x(D_s) < 0.5$ , where a  $b\bar{b}$  contribution is expected. The normalized momentum is defined as  $x(h) = P(h)/P_{max}(h)$ , where  $P(h)$  and  $P_{max}(h)$  are the measured momentum and the maximum possible momentum of particle  $h$ , respectively. Continuum distributions are normalized to  $\Upsilon(5S)$  distributions using the energy corrected luminosity ratio. To extract the number of  $D_s$  events, the candidate mass distribution is fitted to a Gaussian to describe the signal and a linear function to describe the background. The  $x(D_s)$  distributions are shown in Fig. 1b for the  $\Upsilon(5S)$  and continuum data samples. These two distributions agree well in the region  $x(D_s) > 0.5$ , where  $b\bar{b}$  events cannot contribute. An excess of events in the region  $x(D_s) < 0.5$  corresponds to inclusive  $D_s$  production in the  $b\bar{b}$  events.

Subtracting the continuum contribution, applying the efficiency correction, and summing over bins within the interval  $x(D_s) < 0.5$ , the inclusive branching fraction  $\mathcal{B}(\Upsilon(5S) \rightarrow D_s X)/2 = (22.6 \pm 1.2 \pm 2.8)\%$  is obtained. This value is significantly larger than the branching fraction  $\mathcal{B}(B \rightarrow D_s X)$ , which has been measured by the CLEO Collaboration<sup>3</sup> to be  $(9.0 \pm 0.3 \pm 1.4)\%$  and by the BaBar Collaboration<sup>8</sup> to be  $(8.94 \pm 0.16 \pm 1.12)\%$  (corrected for our value of  $\mathcal{B}(D_s^+ \rightarrow \phi\pi^+)$ ). The significant increase of  $D_s$  production at  $\Upsilon(5S)$ , compared with  $\Upsilon(4S)$ , indicates a sizable  $B_s$  production rate.

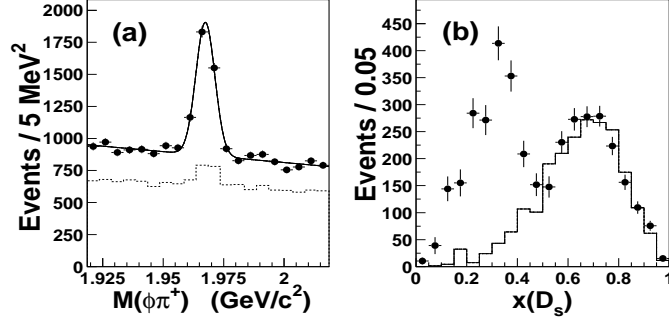


Figure 1: The  $D_s$  signal (a) at the region  $x(D_s) < 0.5$  for the  $\Upsilon(5S)$  (full circles with error bars) and continuum (hatched histogram) data samples, and the  $D_s$  normalized momentum distributions (b) for the  $\Upsilon(5S)$  (full circles with error bars) and continuum (hatched histogram) data samples are shown.

The ratio  $f_s$  of  $B_s^{(*)}\bar{B}_s^{(*)}$  events to all  $b\bar{b}$  events at the  $\Upsilon(5S)$  can be obtained from equation:

$$\mathcal{B}(\Upsilon(5S) \rightarrow D_s X)/2 = f_s \cdot \mathcal{B}(B_s \rightarrow D_s X) + (1 - f_s) \cdot \mathcal{B}(B \rightarrow D_s X) \quad (2)$$

Using  $\mathcal{B}(B_s \rightarrow D_s X) = (92 \pm 11)\%$  obtained in the reference<sup>3</sup> in a model dependent way the value  $f_s = (16.4 \pm 1.4 \pm 4.1)\%$  is obtained from Eq. (2). This value agrees well with  $f_s = (16.0 \pm 2.6 \pm 5.8)\%$  obtained by the CLEO collaboration<sup>3</sup> from the  $D_s$  inclusive analysis. The dominant contributions to systematic uncertainty are the uncertainty on  $\mathcal{B}(D_s^+ \rightarrow \phi\pi^+)$ , the uncertainty on the number of  $b\bar{b}$  events and the uncertainty on the model dependent assumption for  $\mathcal{B}(B_s \rightarrow D_s X)$ .

#### 4 Inclusive $D^0$ and $J/\psi$ Production

The inclusive production of  $D^0$  mesons at the  $\Upsilon(5S)$  is studied in the decay mode  $D^0 \rightarrow K^-\pi^+$  (Fig. 2a,b). Large  $D^0$  signals are seen in Fig. 2a for the  $\Upsilon(5S)$  and continuum data samples for the normalized momentum region  $x(D^0) < 0.5$ . The number of  $D^0$  mesons as a function of the normalized momentum  $x(D^0)$  is shown in Fig. 2b for the  $\Upsilon(5S)$  and continuum data samples. In a manner similar to the  $D_s$  inclusive analysis, the inclusive branching fraction  $\mathcal{B}(\Upsilon(5S) \rightarrow D^0 X)/2 = (53.3 \pm 2.0 \pm 2.9)\%$  is determined. Using the inclusive  $D^0$  production branching fraction of the  $\Upsilon(5S)$ ,  $B$ , and  $B_s$  decays and replacing  $D_s$  by  $D^0$  in Eq.(2), the ratio  $f_s = (18.7 \pm 3.6 \pm 6.7)\%$  of  $B_s^{(*)}\bar{B}_s^{(*)}$  events to all  $b\bar{b}$  events at the  $\Upsilon(5S)$  is obtained. This value agrees with our  $D_s$  measurement.

The inclusive production of  $J/\psi$  mesons is studied in the decay mode  $J/\psi \rightarrow \mu^+\mu^-$  (Fig. 2c,d). The  $J/\psi$  production at the  $\Upsilon(5S)$  can be estimated in a way similar to that used in the inclusive  $D_s$  analysis. In the region  $x(J/\psi) < 0.5$  a prominent  $J/\psi$  signal (Fig. 2c) is seen for the  $\Upsilon(5S)$

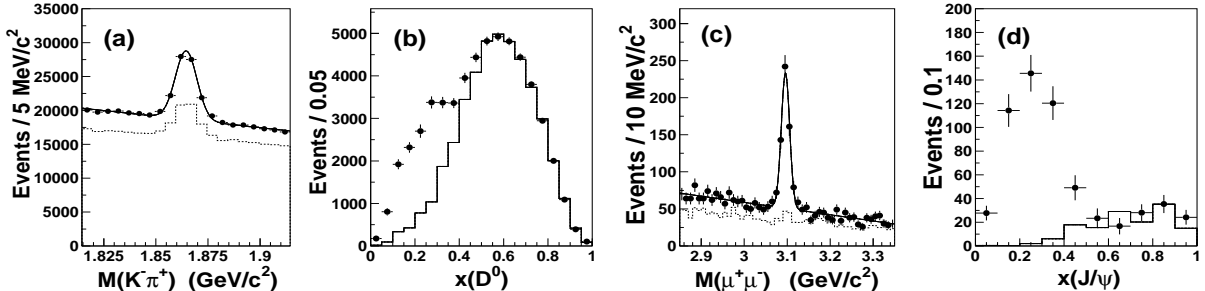


Figure 2: The  $D^0$  (a) and  $J/\psi$  (c) signals at the region  $x < 0.5$  for the  $\Upsilon(5S)$  (full circles with error bars) and continuum (hatched histogram) data samples, and the  $D^0$  (b) and  $J/\psi$  (d) normalized momentum distributions for the  $\Upsilon(5S)$  (full circles with error bars) and continuum (hatched histogram) data samples are shown.

data sample, whereas the  $J/\psi$  signal in continuum is small. The  $J/\psi$  normalized momentum distributions are shown in Fig. 2d for the  $\Upsilon(5S)$  and continuum data samples.

Using the PDG value  $\mathcal{B}(J/\psi \rightarrow \mu^+\mu^-) = (5.88 \pm 0.10)\%$ , the inclusive branching fraction  $\mathcal{B}(\Upsilon(5S) \rightarrow J/\psi X)/2 = (1.068 \pm 0.086 \pm 0.057)\%$  is obtained by summing events in the background subtracted and efficiency corrected  $J/\psi$  normalized momentum distribution. The  $\Upsilon(5S)$  branching fraction can be compared to the  $B$  decay branching fraction  $\mathcal{B}(B \rightarrow J/\psi X) = (1.094 \pm 0.032)\%$ , because the inclusive  $J/\psi$  production rate in  $B$  and  $B_s$  decays is expected to be approximately equal.

## 5 Exclusive $B_s \rightarrow D_s^{(*)+}\pi^-$ , $B_s \rightarrow D_s^{(*)+}\rho^-$ and $B_s \rightarrow J/\Psi\phi(/ \eta)$ Decays

In this analysis we studied the six conventional  $B_s$  decay modes  $B_s \rightarrow D_s^+\pi^-$ ,  $B_s \rightarrow D_s^{*+}\pi^-$ ,  $B_s \rightarrow D_s^+\rho^-$ ,  $B_s \rightarrow D_s^{*+}\rho^-$ ,  $B_s \rightarrow J/\Psi\phi$  and  $B_s \rightarrow J/\Psi\eta$ , which have large reconstruction efficiencies and are described by unsuppressed conventional tree diagrams.  $D_s^+$  mesons are reconstructed in the  $\phi\pi^+$ ,  $\bar{K}^{*0}K^+$  and  $K_S^0K^+$  decay channels. To suppress continuum background we exploit topological cuts.

The signals can be observed using two variables: the energy difference  $\Delta E = E_{B_s}^{CM} - E_{\text{beam}}^{CM}$  and beam-constrained mass  $M_{\text{bc}} = \sqrt{(E_{\text{beam}}^{CM})^2 - (p_{B_s}^{CM})^2}$ ;  $E_{B_s}^{CM}$  and  $p_{B_s}^{CM}$  are the energy and momentum of the  $B_s$  candidate in the  $e^+e^-$  center-of-mass (CM) system and  $E_{\text{beam}}^{CM}$  is the CM beam energy. The  $B_s$  mesons can be produced at the  $\Upsilon(5S)$  energy via the intermediate  $e^+e^- \rightarrow B_s^{(*)}\bar{B}_s^{(*)}$  channels, with  $B_s^* \rightarrow B_s\gamma$ . Most  $B_s$  signal events are concentrated within the ellipsoidal regions, which are kinematically well separated for the  $B_s^*\bar{B}_s^*$ ,  $B_s^*\bar{B}_s$ ,  $B_s\bar{B}_s^*$  and  $B_s\bar{B}_s$  channels.

The distribution of data in  $M_{\text{bc}}$  and  $\Delta E$  for the  $B_s \rightarrow D_s^+\pi^-$  decay mode is shown in Fig. 3a. Nine events are observed within the  $B_s$  signal ellipsoidal region corresponding to  $B_s^*\bar{B}_s^*$  pair production channel. Background outside the signal regions is small. The  $M_{\text{bc}}$  and  $\Delta E$  scatter plots are also obtained for the  $B_s \rightarrow D_s^{*+}\pi^-$  (Fig. 3b),  $B_s \rightarrow D_s^{*+}\rho^-$  (Fig. 3c) and  $B_s \rightarrow J/\Psi\phi(/ \eta)$  (Fig. 3d) decays. One of the observed  $B_s \rightarrow J/\Psi\phi$  candidates is reconstructed in the  $J/\Psi \rightarrow \mu^+\mu^-$  mode and one in the  $J/\Psi \rightarrow e^+e^-$  mode. One candidate is observed in the  $J/\Psi\eta$  decay mode.

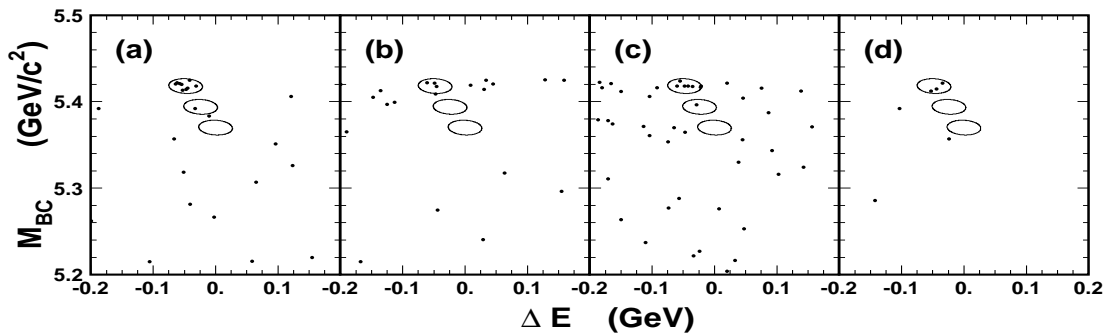


Figure 3: The  $M_{\text{bc}}$  and  $\Delta E$  scatter plots for the  $B_s \rightarrow D_s^+\pi^-$  (a),  $B_s \rightarrow D_s^{*+}\pi^-$  (b) and  $B_s \rightarrow D_s^{*+}\rho^-$  (c) and  $B_s \rightarrow J/\Psi\phi(/ \eta)$  (d) decay modes are shown.

The six  $B_s$  modes shown in Fig. 3 are combined to increase the statistical significance of the  $B_s$  signal. Distributions in  $\Delta E$  are obtained separately for events from three  $M_{\text{bc}}$  intervals, corresponding to  $B_s$  production proceeding through the  $B_s^*\bar{B}_s^*$ ,  $B_s^*\bar{B}_s + B_s\bar{B}_s^*$  or  $B_s\bar{B}_s$  channels, respectively. Each of these three distributions is fitted by the sum of a Gaussian to describe the signal and a linear function to describe background. The fits yield  $20.0 \pm 4.8$  events and

$1.3 \pm 2.0$  events for the  $B_s^* \bar{B}_s^*$  and  $B_s^* \bar{B}_s + B_s \bar{B}_s^*$  channels, respectively; no events are observed in the  $B_s \bar{B}_s$  channel. From these numbers we obtain the ratio  $\sigma(e^+e^- \rightarrow B_s^* \bar{B}_s^*)/\sigma(e^+e^- \rightarrow B_s^{(*)} \bar{B}_s^{(*)}) = 0.94_{-0.09}^{+0.06}$  at the  $\Upsilon(5S)$  energy. Potential models<sup>9,10</sup> predict the fraction of  $B_s^* \bar{B}_s^*$  channel over all these channels to be around 70%.

The  $B_s$  and  $B_s^*$  masses can be extracted from the  $M_{bc}$  fits in the  $B_s^* \bar{B}_s^*$  channel, selecting candidates within the  $-0.08 < \Delta E < -0.02$  MeV range. The  $M_{bc}$  distribution (Fig. 4a) is fitted by the sum of a Gaussian to describe the signal and the so-called ARGUS function<sup>11</sup> to describe background. The fit yields the mass value  $M(B_s^*) = (5418 \pm 1) \text{ MeV}/c^2$ . The observed width of the  $B_s^*$  signal is  $(3.6 \pm 0.6) \text{ MeV}/c^2$  and agrees with the value obtained from the MC simulation, which assumes zero natural width.

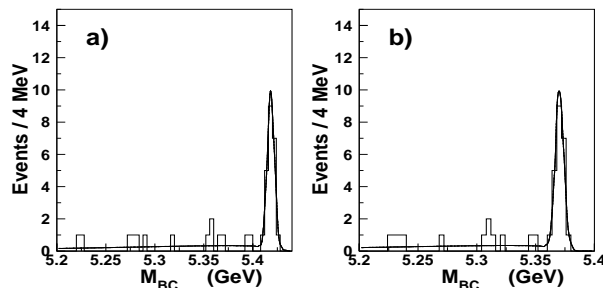


Figure 4: The  $B_s^*$  (a) and  $B_s$  (b) mass distributions for events within the  $-0.08 < \Delta E < -0.02$  MeV interval, corresponding to the  $B_s^* \bar{B}_s^*$  channel. Curves are obtained from the fits described in the text.

Using events from the  $B_s^* \bar{B}_s^*$  channel we can obtain also the  $B_s$  mass (Fig. 4b), replacing the energy  $E_{\text{beam}}^{CM}$  by the term  $E_{\text{beam}}^{CM} - \langle \Delta E \rangle$  in the mass formula. The fit shown in Fig. 4b yields the  $B_s$  mass  $M(B_s) = (5370 \pm 1 \pm 3) \text{ MeV}/c^2$  and width  $\sigma(B_s) = (3.6 \pm 0.6) \text{ MeV}/c^2$ . The second uncertainty in the  $B_s$  mass value is the systematic uncertainty due to the statistical uncertainty on the  $\langle \Delta E \rangle$  measurement. The obtained  $B_s$  mass agrees with the most recent CDF measurement,  $M(B_s) = (5366.0 \pm 0.8) \text{ MeV}/c^2$ .

## 6 Rare $B_s$ Decays

The distributions in data of  $M_{bc}$  and  $\Delta E$  are obtained for reconstructed  $B_s \rightarrow \gamma\gamma$  (Fig. 5a),  $B_s \rightarrow \phi\gamma$  (Fig. 5b),  $B_s \rightarrow K^+K^-$  (Fig. 5c) and  $B_s \rightarrow D_s^{(*)+}D_s^{(*)-}$  (Fig. 5d) candidates. Only the  $B_s$  signal regions corresponding to the dominant  $B_s^* \bar{B}_s^*$  channel are indicated in Fig. 5. These regions are wider for the  $B_s \rightarrow \phi\gamma$  and  $B_s \rightarrow \gamma\gamma$  decays, where the energy losses due to photon radiation lead to a large tail at lower values of  $\Delta E$ .

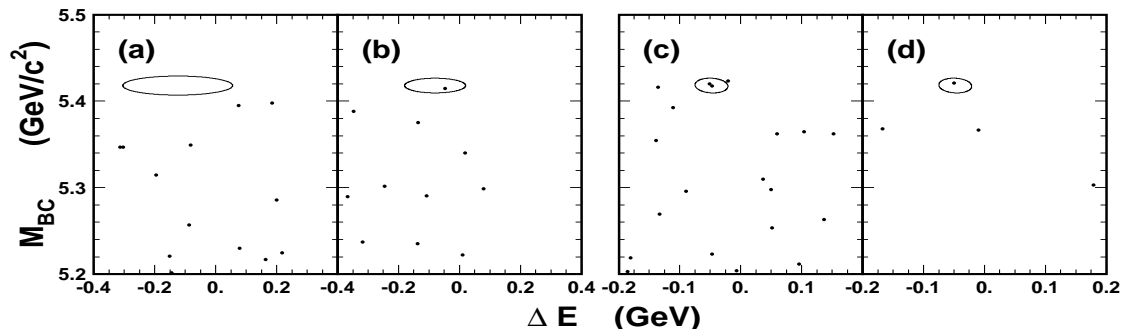


Figure 5: The scatter plots in  $M_{bc}$  and  $\Delta E$  for the  $B_s \rightarrow \gamma\gamma$  (a),  $B_s \rightarrow \phi\gamma$  (b),  $B_s \rightarrow K^+K^-$  (c) and  $B_s \rightarrow D_s^{(*)+}D_s^{(*)-}$  (d) decays. The ellipses are indicating the  $B_s$  signal regions for the  $B_s^* \bar{B}_s^*$  channel.

The numbers of events within the signal regions, estimated background contributions, efficiencies, and upper limits for these decays are listed in Table 1. For comparison, the PDG upper limits are also shown. The number of initial  $B_s^* \bar{B}_s^*$  pairs is obtained by multiplying the number of  $B_s^{(*)} \bar{B}_s^{(*)}$  pairs defined in the inclusive analysis by the production ratio of  $B_s^* \bar{B}_s^*$  pairs to  $B_s^{(*)} \bar{B}_s^{(*)}$  pairs obtained in analysis of conventional exclusive  $B_s$  decays. The efficiencies are determined from MC simulation.

Table 1: The number of events in the signal region, estimated background contribution, efficiencies, upper limits and PDG upper limits for the  $B_s \rightarrow \gamma\gamma$ ,  $B_s \rightarrow \phi\gamma$ ,  $B_s \rightarrow K^+K^-$  and  $B_s \rightarrow D_s^{(*)+}D_s^{(*)-}$  decay modes.

Decay mode	Yield, ev.	Backg., ev.	Eff. (%)	$UL$ ( $10^{-4}$ )	PDG $UL$ ( $10^{-4}$ )
$B_s \rightarrow \gamma\gamma$	0	0.5	20.0	0.56	1.48
$B_s \rightarrow \phi\gamma$	1	0.15	5.9	4.1	1.2
$B_s \rightarrow K^+K^-$	2	0.14	9.5	3.4	0.59
$B_s \rightarrow D_s^+D_s^-$	0	0.02	0.020	710.	-
$B_s \rightarrow D_s^{*+}D_s^-$	1	0.01	0.0099	1270.	-
$B_s \rightarrow D_s^{*+}D_s^{*-}$	0	<0.01	0.0052	2730.	-

The obtained upper limit for the  $B_s \rightarrow \gamma\gamma$  decay is about three times smaller, than the current best world value. Within the Standard Model this decay is expected to proceed via an intrinsic penguin diagram<sup>12</sup> and the branching fraction is expected to be  $(0.5 - 1.0) \times 10^{-6}$ . However that branching fraction is sensitive to some Beyond Standard Model (BSM) contributions and can be higher by one to two orders of magnitude in some BSM models<sup>13,14</sup>. Important results can be obtained using the  $B_s \rightarrow D_s^{(*)+}D_s^{(*)-}$  decay modes<sup>15</sup>. These modes are expected to be predominantly  $CP$  eigenstates and, because of expected large branching fractions, should lead to a sizable lifetime difference between  $CP$ -odd and  $CP$ -even  $B_s$  mesons. Assuming the sum of these branching fractions to be around (5-8)%, we can expect about 5 events in each of four possible final states with statistics of  $\sim 30 \text{ fb}^{-1}$ . Within the SM framework such measurement can provide an important constraint on the value of  $\Delta\Gamma_s/\Gamma_s$ .

## Acknowledgments

We gratefully acknowledge NSF award number PHY-0611671 for travel support.

## References

1. A.F. Falk and A.A. Petrov, *Phys. Rev. Lett.* **85**, 252 (2000).
2. D. Atwood and A. Soni, *Phys. Lett. B* **533**, 37 (2002).
3. CLEO Collaboration, M. Artuso *et al.*, hep-ex/0508047.
4. CLEO Collaboration, G. Bonvicini *et al.*, *Phys. Rev. Lett.* **96**, 022002 (2006).
5. Belle Collaboration, A. Abashian *et al.*, *Nucl. Instrum. Methods A* **479**, 117 (2002).
6. S. Kurokawa and E. Kikutani, *Nucl. Instrum. Methods A* **499**, 1 (2003).
7. Particle Data Group, S. Eidelman *et al.*, *Phys. Lett. B* **592**, 1 (2004).
8. BaBar Collaboration, B. Aubert *et al.*, *Phys. Rev. D* **65**, 091104 (2002).
9. D.M.J. Lovelock *et al.*, *Phys. Rev. Lett.* **54**, 377 (1985).
10. J. Lee-Franzini *et al.*, *Phys. Rev. Lett.* **65**, 2947 (1990).
11. ARGUS Collaboration, H. Albrecht *et al.*, *Phys. Lett. B* **229**, 304 (1989).
12. L. Reina, G. Ricciardi, A. Soni, *Phys. Rev. D* **56**, 5805 (1997).
13. A. Gemintern, S. Bar-Shalom, G. Eilam, *Phys. Rev. D* **70**, 035008 (2004).
14. W. J. Huo, C. D. Lu, Z. J. Xiao, hep-ph/0302177.
15. I. Dunietz, R. Fleischer, U. Nierste, *Phys. Rev. D* **63**, 114015 (2001).